Pair Density Waves from Local Band Geometry

Guodong Jiang and Yafis Barlas
Department of Physics, University of Nevada, Reno, Reno, Nevada 89502, USA

(Received 23 November 2022; revised 27 March 2023; accepted 18 May 2023; published 6 July 2023)

A band-projection formalism is developed for calculating the superfluid weight in two-dimensional multiorbital superconductors with an orbital-dependent pairing. It is discovered that, in this case, the band geometric superfluid stiffness tensor can be locally nonpositive definite in some regions of the Brillouin zone. When these regions are large enough or include nodal singularities, the total superfluid weight becomes nonpositive definite due to pairing fluctuations, resulting in the transition of a BCS state to a pair density wave (PDW). This geometric BCS-PDW transition is studied in the context of two-orbital superconductors, and proof of the existence of a geometric BCS-PDW transition in a generic topological flat band is established.

DOI: 10.1103/PhysRevLett.131.016002

Introduction.—The superfluid weight of a superconductor is proportional to the density and inversely proportional to the effective mass [1]. Since it is the second-order expansion of the superconducting free energy in the center-of-mass momenta (CMM) of Cooper pairs, a positive definite superfluid weight ensures that zero CMM, the BCS state, minimizes the superconducting free energy. This stability criterion is also satisfied by the recently discovered geometric superfluid weight in multiorbital superconductors, which is proportional to the quantum metric of the band [2–17]. It is positive semidefinite for an orbital-independent order parameter [18], and dominates in flat band superconductors like twisted or strained two-dimensional (2D) crystals [19–32]. These rigid stability criteria seemingly preclude the existence of a pair density wave (PDW) state, which is an exotic superconductor whose electron pairs condense with a nonzero CMM [33–40].

In this Letter, we show that the band geometric effect can stabilize a PDW state in flat bands with orbital-dependent pairing. Our analysis is based on the understanding of pairing instabilities that result from a negative definite superfluid weight $D_{s,\mu\nu}$ in multiorbital superconductors. This criterion has recently been used to study the Fulde-Ferrell-Larkin-Ovchinnikov state in magnetic fields [41] and PDW states [42]. However, the transition mechanism and its nature remain shrouded in mystery. Our theory, aided by developing a band-projection formalism for the superfluid weight, allows us to identify a unique nodal mechanism that drives a BCS-PDW transition in the presence of orbital-dependent pairing. In the process, we establish an intimate connection between band topology and the BCS-PDW transition in superconductors.

The nodal mechanism requires the presence of zeros in the quasiparticle spectrum. When these zeros coincide with the negative contributions to the superfluid weight ($D_{s,\mu\nu}$), they dominate over the positive contributions. We show that a topological two-orbital band always exhibits at least one nodal zero in the quasiparticle spectrum. Above a critical coupling, $D_{s,\mu\nu}$ becomes negative definite in the neighborhood of this nodal zero, driving a second-order BCS-PDW transition [43]. To justify our claims with an explicit example, we study the BCS-PDW transitions in the flattened Bernevig-Hughes-Zhang (BHZ) model [44,45]. The PDW phase corresponds to the simultaneous presence of an attractive and repulsive channel, with the transition initiated by one channel turning repulsive. Below we sketch the analysis that leads to these results.

Projected superfluid weight.—We begin by describing our formalism for calculating the projected superfluid weight of multiorbital superconductors with orbital-dependent pairing. Consider the 2D lattice Hamiltonian

$$\hat{\mathcal{H}} = \sum_{ij,\alpha\beta,\sigma} h^{\sigma}_{ij,\alpha\beta} c^{\dagger}_{i\alpha\sigma} c_{j\beta\sigma} - \sum_{i,\alpha\beta} U_{\alpha\beta} c^{\dagger}_{i\alpha\uparrow} c^{\dagger}_{i\beta\downarrow} c_{i\beta\downarrow} c_{i\alpha\uparrow}, \quad (1)$$

where i, j denote the Bravais lattice site, $\sigma = \uparrow, \downarrow$ the spin, and α, β orbitals or internal degrees of freedom other than spin. The generic single-particle Hamiltonian $h^{\sigma}_{ij,\alpha\beta}$ captures the hoppings between orbital (i,α) and (j,β), where the spin-orbit coupling is ignored. The on-site pairing interaction $U_{\alpha\beta}$ is orbital-dependent and limited to singlet pairing. We assume that the Fermi energy μ lies within the mth band with spin-$\uparrow$ Bloch function $u_{m,\boldsymbol{k}}$ and energy $\varepsilon_{m,\boldsymbol{k}}$. Furthermore, to justify band projection, we assume that the interaction strength is of the order of bandwidth and much smaller than the band gap, $\delta\varepsilon_{m,\boldsymbol{k}} \lesssim |U_{\alpha\beta}| \ll E_{\mathrm{gap}}$.

The superfluid weight tensor encodes the stability to the pairing fluctuation of $\boldsymbol{k}+\boldsymbol{q}, \uparrow$ and $-\boldsymbol{k}+\boldsymbol{q}, \downarrow$ electrons [46]. For stability, it must be positive definite (PD). We perform the usual mean-field decoupling to arrive at the

Bogoliubov–de Genne Hamiltonian $\hat{\mathcal{H}}_{\rm MF}(\hat{\Delta}) - \mu\hat{N}_e$, where $\hat{N}_e$ is the total electron number operator. The mean-field order parameter $\hat{\Delta}_{\alpha\beta} = -U_{\alpha\beta}\langle c_{i\beta\downarrow}c_{i\alpha\uparrow}\rangle$ must be attained self-consistently (see Supplemental Material [47]). The projected grand potential for the mth band, $\Omega_m(\boldsymbol{q})$, can be expressed as

$$\Omega_m(\boldsymbol{q}) = -\frac{1}{\beta}\ln \mathrm{tr}\left\{ e^{-\beta\hat{\mathcal{P}}_m(\boldsymbol{q})[\hat{\mathcal{H}}_{\rm MF}(\hat{\Delta}_{\boldsymbol{q}}) - \mu_{\boldsymbol{q}}\hat{N}_e]\hat{\mathcal{P}}_m(\boldsymbol{q})} \right\}, \quad (2)$$

where $\hat{\mathcal{P}}_m(\boldsymbol{q})$ is a $\boldsymbol{q}$-dependent band-projection operator, and $\mu_{\boldsymbol{q}}$, $\hat{\Delta}_{\boldsymbol{q}}$ are self-consistency functions coming from particle number constraint and the gap equation [2,48] (see Supplemental Material [47]).

To calculate the mth-band projected superfluid weight, $D^m_{s,\mu\nu}$, we assume that the translationally invariant BCS state is an extremum of the free energy. This is guaranteed when $\hat{\Delta}$ is Hermitian [49], giving $\widetilde{\partial}_{q_\mu}|\Delta_{m,\boldsymbol{k}}(\boldsymbol{q})|^2|_{\boldsymbol{q}=0} = 0$, where

$$\Delta_{m,\boldsymbol{k}}(\boldsymbol{q}) = \langle u_{m,\boldsymbol{k}+\boldsymbol{q}}|\hat{\Delta}_{\boldsymbol{q}}|u_{m,\boldsymbol{k}-\boldsymbol{q}}\rangle \quad (3)$$

is the band-projected gap function and symbol $\widetilde{\partial}_{q_\mu}$ means the derivative does not act on $\mu_{\boldsymbol{q}}$ or $\hat{\Delta}_{\boldsymbol{q}}$, with $\mu = x, y$. Here, we focus on 2D systems at zero temperature; the finite-temperature case will be discussed elsewhere. The superfluid weight is computed from $D^m_{s,\mu\nu} = (1/N)\widetilde{\partial}_{q_\mu}\widetilde{\partial}_{q_\nu}\Omega_m(\boldsymbol{q})|_{\boldsymbol{q}=0}$, where $\hbar$ and the unit cell area have been set to 1, and N is the number of unit cells. At $T = 0$, it can be expressed as $D^m_{s,\mu\nu} = D^{m,\mathrm{conv}}_{s,\mu\nu} + D^{m,\mathrm{geo}}_{s,\mu\nu}$,

$$D^{m,\mathrm{conv}}_{s,\mu\nu} = \frac{1}{N}\sum_{\boldsymbol{k}}\left(1 - \frac{\xi_{m,\boldsymbol{k}}}{E_{m,\boldsymbol{k}}}\right)\partial_\mu\partial_\nu\xi_{m,\boldsymbol{k}}, \quad (4)$$

$$D^{m,\mathrm{geo}}_{s,\mu\nu} = \frac{1}{N}\sum_{\boldsymbol{k}}\frac{G^m_{\mu\nu}(\boldsymbol{k})}{2E_{m,\boldsymbol{k}}}, \quad (5)$$

where $G^m_{\mu\nu}(\boldsymbol{k}) \equiv -\widetilde{\partial}_{q_\mu}\widetilde{\partial}_{q_\nu}|\Delta_{m,\boldsymbol{k}}(\boldsymbol{q})|^2|_{\boldsymbol{q}=0}$ is a gauge-invariant quantity that depends on both the Bloch function $u_{m,\boldsymbol{k}}$ and pairing matrix $\hat{\Delta}$, $\xi_{m,\boldsymbol{k}} = \varepsilon_{m,\boldsymbol{k}} - \mu$, and $E_{m,\boldsymbol{k}} = \sqrt{\xi^2_{m,\boldsymbol{k}} + |\Delta_{m,\boldsymbol{k}}(0)|^2}$. The conventional superfluid weight, $D^{m,\mathrm{conv}}_{s,\mu\nu}$, is proportional to the band curvature and vanishes in the flat band limit. The generalized geometric superfluid weight, $D^{m,\mathrm{geo}}_{s,\mu\nu}$, depends on the Bloch function $u_{m,\boldsymbol{k}}$ through $G^m_{\mu\nu}$, which captures the band geometry.

When $\hat{\Delta} = \Delta_0\hat{\mathcal{I}}$, we find $G^m_{\mu\nu}(\boldsymbol{k}) = 8|\Delta_0|^2 g^m_{\mu\nu}(\boldsymbol{k})$, where $g^m_{\mu\nu}(\boldsymbol{k})$ is the quantum metric of the mth band, defined as the real part of quantum geometric tensor $R^m_{\mu\nu}(\boldsymbol{k}) = \langle\partial_\mu u_{m,\boldsymbol{k}}|(1 - |u_{m,\boldsymbol{k}}\rangle\langle u_{m,\boldsymbol{k}}|)|\partial_\nu u_{m,\boldsymbol{k}}\rangle$ [50]. This quantum-metric contribution was previously reported [2,4] and is always PD. However, for a general pairing matrix $\hat{\Delta}$, tensor $G^m_{\mu\nu}(\boldsymbol{k})$ may be locally *nonpositive definite* (NPD).

It is important to note that while $G^m_{\mu\nu}(\boldsymbol{k})$ is determined by the local band geometry and pairing matrix $\hat{\Delta}$, $D^{m,\mathrm{geo}}_{s,\mu\nu}$, which determines the stability criteria, depends on both the band geometry and the quasiparticle spectrum $E_{m,\boldsymbol{k}}$. This gives an intriguing admixture of band geometry and energetics. We find that the NPD behavior of $G^m_{\mu\nu}(\boldsymbol{k})$, even in part of the Brillouin zone (BZ), can make $D^m_{s,\mu\nu}$ NPD, resulting in the pairing instability.

Instability toward a PDW state.—To understand the physics associated with $D^{m,\mathrm{geo}}_{s,\mu\nu}$, we analyze $G^m_{\mu\nu}(\boldsymbol{k})$ for a two-band system. We assume the order parameter matrix $\hat{\Delta} = \Delta_0\hat{\mathcal{I}} + \Delta_z\hat{\sigma}_z$, where Δ_0, Δ_z are real and $\hat{\sigma}_z$ is the Pauli matrix on orbitals. This is equivalent to setting $U_{\alpha\beta} = \mathrm{diag}(U_{11}, U_{22})$ in the self-consistency equations. For a two-band Bloch Hamiltonian, $h^{\uparrow}(\boldsymbol{k}) = \boldsymbol{h}(\boldsymbol{k})\cdot\boldsymbol{\sigma}$ with $\boldsymbol{h}(\boldsymbol{k}) = [h_x(\boldsymbol{k}), h_y(\boldsymbol{k}), h_z(\boldsymbol{k})]$,

$$G^{v(c)}_{\mu\nu}(\boldsymbol{k}) = 2\Delta_0^2\partial_\mu\hat{\boldsymbol{h}}\cdot\partial_\nu\hat{\boldsymbol{h}} \mp 2\Delta_0\Delta_z\partial_\mu\partial_\nu\hat{h}_z - 2\Delta_z^2(\partial_\mu\hat{h}_x\partial_\nu\hat{h}_x + \partial_\mu\hat{h}_y\partial_\nu\hat{h}_y + \hat{h}_z\partial_\mu\partial_\nu\hat{h}_z), \quad (6)$$

where $\hat{\boldsymbol{h}} = \boldsymbol{h}/|\boldsymbol{h}|$ and $v(c)$ denotes the valance (conduction) band. As noted above, the Δ_0^2 term contains the quantum-metric contribution, $g_{\mu\nu}(\boldsymbol{k}) = (1/4)\partial_\mu\hat{\boldsymbol{h}}\cdot\partial_\nu\hat{\boldsymbol{h}}$. This PD term competes with the NPD contributions associated with $\Delta_0\Delta_z$ and Δ_z^2 terms. It is easy to generalize Eq. (6) for a Hermitian $\hat{\Delta}$ (see Supplemental Material [47]).

When the $\boldsymbol{k}$-space integral of the NPD contributions in Eq. (5) dominates, $D^{m,\mathrm{geo}}_{s,\mu\nu}$ becomes NPD (see Fig. 1) and the BCS state no longer minimizes the free energy. Since

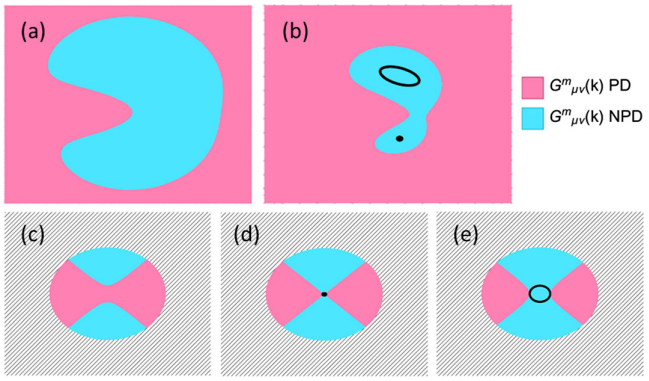

FIG. 1. (a),(b) Schematic representations of two mechanisms leading to a NPD $D^{m,\mathrm{geo}}_{s,\mu\nu}$. In (a), the $G^m_{\mu\nu}$ NPD region dominates over the PD region in the BZ, and in (b), the NPD $G^m_{\mu\nu}$ region encloses nodal points or circles. These singularities dominate even when the NPD area is small. (c)–(e) NPD $D^{m,\mathrm{geo}}_{s,\mu\nu}$ driven by nodal circles for a generic topological flat band with (c) $\Delta_z/\Delta_0 \lesssim 1$, (d) $\Delta_z/\Delta_0 = 1$, (e) $\Delta_z/\Delta_0 \gtrsim 1$. Only the neighborhood of a nodal point is shown explicitly, while the rest of BZ is shaded.

the free energy is defined over a compact domain of $\boldsymbol{q}$, it must attain an energy minimum at some $\boldsymbol{Q} \neq 0$, resulting in transitions to a PDW state. To estimate the transition point, consider a general class of two-band Hamiltonians: $h_z(\boldsymbol{k}) \to M$, with $M \gg |h_x|, |h_y|$. In a "quasiflat" band limit, defined by condition $|\partial_\mu \partial_\nu (h_x^2 + h_y^2)| \ll |\partial_\mu h_x \partial_\nu h_x|$, $|\partial_\mu h_y \partial_\nu h_y|$, $G_{\mu\nu}(\boldsymbol{k})$ becomes

$$G_{\mu\nu}(\boldsymbol{k}) \approx \frac{2(\Delta_0^2 - \Delta_z^2)}{M^2} (\partial_\mu h_x \partial_\nu h_x + \partial_\mu h_y \partial_\nu h_y), \quad (7)$$

which is negative semidefinite for $|\Delta_z/\Delta_0| \geq 1$, giving a NPD $D_{s,\mu\nu}^{m,\mathrm{geo}}$. Therefore, $|\Delta_z/\Delta_0| \geq 1$ indicates the transition to PDW state. As shown in Fig. 1(a), when the integrand of Eq. (5) is a regular function over the BZ, this transition occurs when the NPD contributions (blue regions) dominate the PD contributions (red regions).

PDW driven by nodal singularities.—A more interesting scenario occurs in the presence of nodal zeroes (points or arcs) in the quasiparticle spectrum $E_{m,\boldsymbol{k}}$. When these nodal zeroes are contained in the nonvanishing NPD regions of $G_{\mu\nu}^m$ in the BZ, as shown in Fig. 1(b), $D_{\mu\nu}^{m,\mathrm{geo}}$ becomes singular and NPD. Analysis of nodal singularities shows that such a divergence requires $E_{m,\boldsymbol{k}} \propto k^\alpha$ with $\alpha \geq 2$ near nodal points and $\alpha \geq 1$ near nodal arcs, where k is the distance from $\boldsymbol{k}$ to the nodal point or arc. In this case, the conventional superfluid weight, which is always regular, can be ignored, indicating that the BCS-PDW transition will occur as long as the NPD regions of $G_{\mu\nu}^m$ enclose these nodal zeroes.

The valence-band-projected order parameter for $\hat{\Delta} = \Delta_0 \hat{\mathcal{I}} + \Delta_i \hat{\sigma}_i$ can be calculated from Eq. (3), giving $\Delta_{v,\boldsymbol{k}} = \Delta_0 - \Delta_i \hat{h}_i(\boldsymbol{k})$, where $i = x, y, z$. In a flat band, when $\Delta_i = \Delta_0$, an isolated nodal point appears at $\boldsymbol{k}_0$ if $\hat{h}_i(\boldsymbol{k}_0) = 1$. If the band is also topological, the map of $\boldsymbol{k} \mapsto \hat{\boldsymbol{h}}(\boldsymbol{k})$ wraps the entire Bloch sphere; *hence a nodal point singularity is always present at* $\Delta_i = \pm\Delta_0$, *for any hybridization direction* i. Near the nodal point $\boldsymbol{k}_0$, $G_{xx}^v(\boldsymbol{k})$ for the case $i = z$ can be expanded as

$$G_{xx}^v(\boldsymbol{k}) \approx -v^2 \Delta_0^2 \{v^2(p_y^2 - p_x^2) + 2\eta[1 + v^2(p_y^2 + p_x^2)]\} \quad (8)$$

to the leading order in η, where $\boldsymbol{p} = \boldsymbol{k} - \boldsymbol{k}_0$, $\eta = g - 1$ with $g = \Delta_z/\Delta_0$, and $v > 0$ is an expansion coefficient (see Supplemental Material [47]). At $g = 1$, the nodal point is regular since $G_{\mu\nu}^v(\boldsymbol{k}) \to 0$ [Fig. 1(d)]. However, when $g \gtrsim 1$, the nodal point expands to a circle, which is contained in the NPD $G_{\mu\nu}^v$ regions [Fig. 1(e)]. This negative singular contribution dominates in the $\boldsymbol{k}$-space integral of Eq. (5), resulting in a negative divergent D_s^v for $g > 1$. Since this behavior is determined from topological considerations, it applies to a generic topological two-band model with a Hermitian pairing matrix $\hat{\Delta}$.

BCS-PDW transition in the BHZ model.—To explore the BCS-PDW transitions in detail, we study the BCS instability in the flattened BHZ model, for a $\hat{\Delta} = \Delta_0 \hat{\mathcal{I}} + \Delta_z \hat{\sigma}_z$. To keep the focus on the geometric term, we flatten the model by taking $h^\uparrow(\boldsymbol{k}) = \epsilon_0 \hat{\boldsymbol{h}} \cdot \boldsymbol{\sigma}$, where $\hat{\boldsymbol{h}}$ is the unit vector proportional to $(\sin k_x, \sin k_y, m_0 + \cos k_x + \cos k_y)$. The band gap $2\epsilon_0$ is assumed to be larger than the interaction energy $U_{\alpha\beta}$, and m_0 is the scaled BHZ mass. Spin-orbit coupling is ignored, so the two spin components are decoupled and related by time-reversal symmetry. The BHZ model has a rich phase diagram with four phases: two topological phases $|m_0| < 2$ with Chern number $C = -\mathrm{sgn}(m_0)$, and two trivial phases $|m_0| > 2$. This flattened Hamiltonian is invalid at the "gapless" phase boundary $m_0 = 0, \pm 2$, where the model undergoes a topological phase transition. For our calculations, we project to the valence band and take μ to be around $-\epsilon_0$.

In the flattened BHZ model, nodal zeroes occur when the projected band gap vanishes. When $\Delta_z/\Delta_0 > 0$, this happens for $m_0 > -2$ phases, where the BCS theory predicts nodal superconductors; for $m_0 < -2$, the superconductor is fully gapped. The three phases—$m_0 > 2$, $0 < m_0 < 2$, and $-2 < m_0 < 0$—have 4, 3, and 1 nodal zeroes, respectively. To cure the divergence, we calculate $D_{s,\mu\nu}^v$ with a small broadening $\xi_{v,\boldsymbol{k}} = \epsilon$ or weak dispersion $\xi_{v,\boldsymbol{k}} = \delta\xi_{\boldsymbol{k}}$ in the quasiparticle energy (see Supplementary Material [47]), hereafter, referred to as ϵ-broadened and dispersion-broadened.

Figures 2(a) and 2(b) show the superfluid weight as a function of $g = \Delta_z/\Delta_0$ in various BHZ phases for the ϵ-broadened and dispersion-broadened cases, respectively. Since σ_z pairing term preserves the C_4 rotation symmetry, $D_{s,xx}^v = D_{s,yy}^v = D_s^v$. At some critical point $g = g_c$, D_s^v

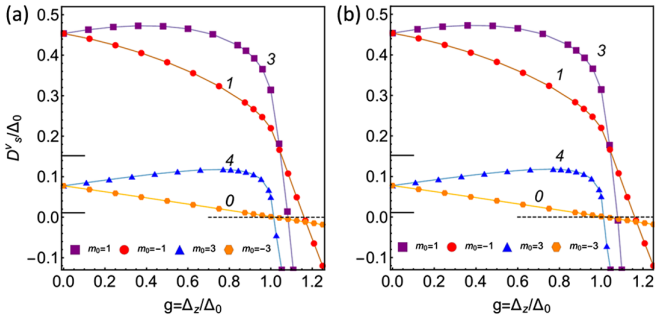

FIG. 2. Superfluid weight D_s^v vs $\Delta_z/\Delta_0 (>0)$ for $\Delta_0 \hat{\mathcal{I}} + \Delta_z \hat{\sigma}_z$ type pairing. Four distinct BHZ phases $m_0 = \pm 1, \pm 3$ are shown, with their number of nodal circles indicated by the numerical values. The horizontal lines indicate the topological lower bound for the two topological and trivial phases. (a) With broadening $\epsilon = 0.01\Delta_0$, $E_{v,\boldsymbol{k}} = \sqrt{\epsilon^2 + |\Delta_{v,\boldsymbol{k}}(0)|^2}$. (b) With weak dispersion of bandwidth $\delta\xi_{\boldsymbol{k}} \sim 0.01\Delta_0$, $E_{v,\boldsymbol{k}} = \sqrt{\delta\xi_{\boldsymbol{k}}^2 + |\Delta_{v,\boldsymbol{k}}(0)|^2}$. In this case, the conventional superfluid weight [Eq. (4)] is also included.

becomes negative, indicating a transition to the PDW state. The four values of $m_0 = \pm 1, \pm 3$ represent the distinct BHZ phases. The horizontal black lines indicate the lower bound for D_s^v at $\Delta_z = 0$, where the quantum metric is lower-bounded by the absolute value of Berry curvature [2]. For this reason, the topological phases $m_0 = \pm 1$ have larger D_s^v than the trivial phases $m_0 = \pm 3$ at small g values.

In Figs. 2(a) and 2(b), the superfluid weight for the $m_0 = 3, \pm 1$ phases is marked by a sharp downturn of D_s^v near $g = 1$. This behavior can be attributed to nodal circles of quasiparticle energy $E_{v,\boldsymbol{k}}$ [Figs. 1(c)–1(e)]. We find no qualitative differences between the curves of the ϵ-broadened and dispersion-broadened cases. More nodal circles results in a steeper slope of D_s^v at $g > 1$. In contrast, the $m_0 = -3$ phase has no nodal zeros for $g \geq 1$. Hence D_s^v decreases steadily.

Figure 3 shows the BCS-PDW phase boundary determined from the instability condition $D_s^v = 0$ as a function of m_0. D_s^v becomes negative at $g_c \gtrsim 1$, for all m_0 values, especially $g_c \to 1$ as $m_0 \to \pm\infty$. This asymptotic behavior can be confirmed by an analysis similar to the previous discussion of a "quasiflat" band. Figure 3 also shows the dependence of the phase boundary on ϵ. ϵ-broadening smears the nodal singularities of all three BHZ phases at $m_0 > -2$, requiring a larger g value for the PDW transition. The $m_0 < -2$ phase has no nodal zeroes, so the phase boundary is unaffected. A careful examination of the free energy as a function of CMM $\boldsymbol{q}$ shows that the D_s^v instability curves coincide with the BCS-PDW phase boundary only when the transition is second-order. There are also two types of weak first-order transitions located at $m_0 < -2$ and $m_0 > 2.85$, which are slightly below the instability curve. These findings are summarized in Figs. 3(b) and 3(c).

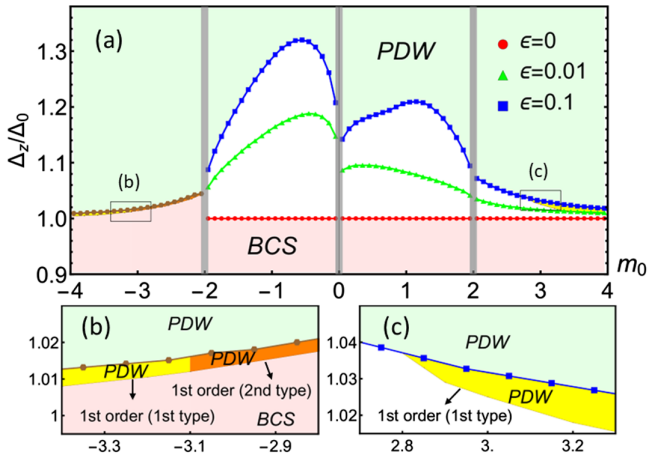

FIG. 3. Phase diagram of the flattened BHZ model with $\Delta_0\hat{\mathcal{I}} + \Delta_z\hat{\sigma}_z$ pairing. (a) D_s^v instability curves for broadening $\epsilon = 0, 0.01$, and 0.1 are shown in red, green, and blue, respectively; they coincide in the $m_0 < -2$ phase so are shown in brown. The $\epsilon = 0$ data for $m_0 > -2$ phases come from nodal singularity analysis. For second-order transitions, these curves are identical to the BCS-PDW phase boundary. The BCS region $0 < \Delta_z/\Delta_0 < 0.9$ is snipped. (b),(c) Magnified plots showing the first-order phase transition details with the same axis labels as (a). $\epsilon = 0.01$ is similar to $\epsilon = 0.1$, so only $\epsilon = 0.1$ data is shown. (b) Two types of first-order transitions, at $-\infty < m_0 < -2$, are separated at $m_0 \sim -3.1$. (c) The first type of first-order transition at $2.85 < m_0 < +\infty$.

Pair density wave.—To understand the nature of the BCS-PDW phase transition and the properties of the PDW state, we calculate the free energy per unit cell, $F_v(\boldsymbol{q})/N$ as a function of the CMM $\boldsymbol{q}$. The free energy is $F_v(\boldsymbol{q}) = \Omega_v(\boldsymbol{q}) + \mu_{\boldsymbol{q}} N_{e,v}$, with $N_{e,v}$ the total electron number in the valence band and $\Omega_v(\boldsymbol{q})$ evaluated from Eq. (2) at $T = 0$ (see Supplemental Material [47] for details). $F_v(\boldsymbol{q})$ has the periodicity of time-reversal-invariant momentum (TRIM), which time-reversal symmetry imposes. Therefore we only need to focus on the region enclosed by Γ (0,0), X $(\pi, 0)$, M (π, π), and X' $(0, \pi)$ in $\boldsymbol{q}$ space. As D_s^v turns negative, these four high symmetry points are no longer local minima of $F_v(\boldsymbol{q})$, and a new minimum at $\boldsymbol{Q}$ corresponding to the CMM of PDW state emerges in the BZ.

In general, the CMM $\boldsymbol{Q}$ is a function of model parameters and depends on the transition type. In continuous models, the transition type may depend on the higher-order derivatives of free energy [41,51]; here in a lattice, it has to be determined from the calculation of $F_v(\boldsymbol{q})$ in all of $\boldsymbol{q}$ space. For our model, C_4 symmetry gives that $\boldsymbol{Q}$ modulo TRIM can be one of the four vectors $\boldsymbol{Q}_i = \{(\pm Q, 0), (0, \pm Q)\}$, giving a set of biaxial PDW orders $\{\Delta_{\boldsymbol{Q}_1}, \Delta_{\boldsymbol{Q}_2}, \Delta_{\boldsymbol{Q}_3}, \Delta_{\boldsymbol{Q}_4}\}$. In Fig. 4, we show three prototypes of BCS-PDW transitions, at parameter $m_0 = 2.5$, 3, and -3, respectively (c.f. Fig. 3). The PDW phase corresponds to $U_{11}U_{22} < 0$, and the BCS-PDW transition coincides with one channel turning repulsive. The full phase diagram in the (U_{11}, U_{22}) parameter space is provided in the Supplemental Material [47].

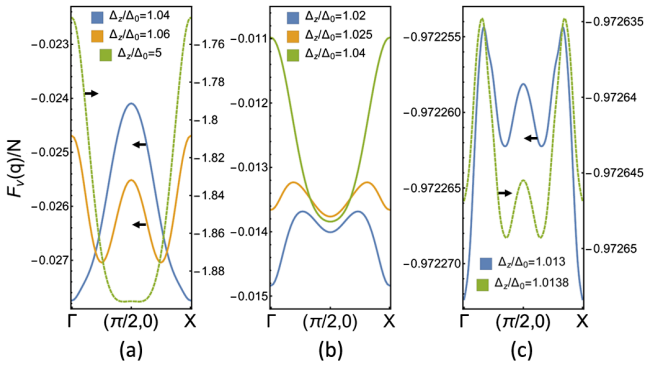

FIG. 4. $F_v(\boldsymbol{q})/N$ (in units of Δ_0) along ΓX in $\boldsymbol{q}$ space, for three types of BCS-PDW transitions. (a) The second-order transition at $\epsilon = 0.1$, $m_0 = 2.5$, $Q \neq \pi/2$; (b) first-order transition (first type) at $\epsilon = 0.1$, $m_0 = 3$, $Q = \pi/2$; (c) first-order transition (second type) at $\epsilon = 0.1$, $m_0 = -3$, $Q \neq \pi/2$.

Second-order transitions [Fig. 4(a)] are found in the middle region $-2 < m_0 < 2.85$ of the phase diagram, with a maximum of free energy appearing at $(\pi/2,\ 0)$. The transition occurs precisely when D_s^v becomes negative, creating two minima $(Q, 0), (\pi - Q, 0)$ on ΓX, resulting in an incommensurate PDW. Notice $(\pi - Q, 0)$ is equivalent to $(-Q, 0)$ by shifting a TRIM. As Δ_z/Δ_0 becomes large, Q tends to $\pi/2$, and the two minima merge into one, possibly converging to a commensurate PDW.

As shown in Figs. 3(b) and 3(c), the BCS-PDW transitions for the flattened BHZ model can also be first order. There are two types of first-order transitions, depending on the presence of minima or maxima at $(\pi/2, 0)$. If it is a minimum [Fig. 4(b)], then $Q = \pi/2$ is a constant and competes with the $\boldsymbol{q} = 0$ BCS state. This first type of first-order transitions is found in the phase diagram's atomic regions $m_0 < -3.1$ or > 2.85, and results in a commensurate PDW. Otherwise, if it is a maximum [Fig. 4(c)], then there are two minima $(Q, 0), (\pi - Q, 0)$ competing with the $\boldsymbol{q} = 0$ state, resulting in an incommensurate PDW. This second type can be viewed as a hybrid of the previous two types of transitions and is located in the intermediate region $-3.1 < m_0 < -2$. As Δ_z/Δ_0 becomes large, $Q \to \pi/2$ is also observed.

Discussion.—The geometric instabilities discussed here are relevant to various weakly dispersive or flat band multiorbital superconductors—for example, alternating twisted-graphene-based superconductors—that exhibit superconducting diode effect [52,53]. In these twisted 2D crystals, spin fluctuations of the interaction-induced Chern bands result in orbital-dependent pairing interactions [54] with a simultaneous attraction and repulsion channel, along with a significant geometric superfluid weight [12–14]. Additionally, twisted transition metal dichalcogenides exhibit topological flat bands on bipartite honeycomb and Kagome Hubbard models [55], where antiferromagnetic spin fluctuations can result in orbital-dependent pairing. On the other hand, the nodal geometric BCS-PDW transition mechanism should apply to dispersive bands. In fact, PDWs have been observed in Kagome [56] and Lieb lattice superconductors [57–59], where the bandwidth is comparable to interactions. The possibility of band geometric instabilities in these multiorbital superconductors is left to future studies.

The authors would like to thank Professor E. Rossi for his comments on the manuscript. Both authors acknowledge support from UNR VPRI startup Grant No. PG19012.

[1] J. Schrieffer, *Theory of Superconductivity*, Advanced Books Classics (Avalon Publishing, Boca Raton, 1999).
[2] S. Peotta and P. Törmä, Nat. Commun. **6**, 8944 (2015).
[3] A. Julku, S. Peotta, T. I. Vanhala, D.-H. Kim, and P. Törmä, Phys. Rev. Lett. **117**, 045303 (2016).
[4] L. Liang, T. I. Vanhala, S. Peotta, T. Siro, A. Harju, and P. Törmä, Phys. Rev. B **95**, 024515 (2017).
[5] M. Iskin, Phys. Rev. A **97**, 063625 (2018).
[6] P. Törmä, L. Liang, and S. Peotta, Phys. Rev. B **98**, 220511 (R) (2018).
[7] Z. Wang, G. Chaudhary, Q. Chen, and K. Levin, Phys. Rev. B **102**, 184504 (2020).
[8] A. Julku, G. M. Bruun, and P. Törmä, Phys. Rev. Lett. **127**, 170404 (2021).
[9] J. Wang, J. Cano, A. J. Millis, Z. Liu, and B. Yang, Phys. Rev. Lett. **127**, 246403 (2021).
[10] E. Rossi, Curr. Opin. Solid State Mater. Sci. **25**, 100952 (2021).
[11] P. Törmä, S. Peotta, and B. A. Bernevig, Nat. Rev. Phys. **4**, 528 (2022).
[12] X. Hu, T. Hyart, D. I. Pikulin, and E. Rossi, Phys. Rev. Lett. **123**, 237002 (2019).
[13] F. Xie, Z. Song, B. Lian, and B. A. Bernevig, Phys. Rev. Lett. **124**, 167002 (2020).
[14] H. Tian, X. Gao, Y. Zhang, S. Che, T. Xu, P. Cheung, K. Watanabe, T. Taniguchi, M. Randeria, F. Zhang, C. N. Lau, and M. W. Bockrath, Nature (London) **614**, 440 (2023).
[15] J. S. Hofmann, E. Berg, and D. Chowdhury, Phys. Rev. B **102**, 201112(R) (2020).
[16] M. Tovmasyan, S. Peotta, P. Törmä, and S. D. Huber, Phys. Rev. B **94**, 245149 (2016).
[17] J. Herzog-Arbeitman, V. Peri, F. Schindler, S. D. Huber, and B. A. Bernevig, Phys. Rev. Lett. **128**, 087002 (2022).
[18] The superfluid weight $D_{s,\mu\nu}$ can be nonpositive definite for particle-hole asymmetric bands, as in the case of exciton condensates. However, for superconductors, the system obeys particle-hole symmetry.
[19] R. Bistritzer and A. H. MacDonald, Proc. Natl. Acad. Sci. U.S.A. **108**, 12233 (2011).
[20] B. Uchoa and Y. Barlas, Phys. Rev. Lett. **111**, 046604 (2013).
[21] B. Uchoa and K. Seo, Phys. Rev. B **96**, 220503(R) (2017).
[22] Y. Cao, V. Fatemi, A. Demir, S. Fang, S. L. Tomarken, J. Y. Luo, J. D. Sanchez-Yamagishi, K. Watanabe, T. Taniguchi, E. Kaxiras, R. C. Ashoori, and P. Jarillo-Herrero, Nature (London) **556**, 80 (2018).
[23] Y. Cao, V. Fatemi, S. Fang, K. Watanabe, T. Taniguchi, E. Kaxiras, and P. Jarillo-Herrero, Nature (London) **556**, 43 (2018).
[24] X. Lu, P. Stepanov, W. Yang, M. Xie, M. A. Aamir, I. Das, C. Urgell, K. Watanabe, T. Taniguchi, G. Zhang, A. Bachtold, A. H. MacDonald, and D. K. Efetov, Nature (London) **574**, 653 (2019).
[25] A. L. Sharpe, E. J. Fox, A. W. Barnard, J. Finney, K. Watanabe, T. Taniguchi, M. A. Kastner, and D. Goldhaber-Gordon, Science **365**, 605 (2019).
[26] M. Yankowitz, S. Chen, H. Polshyn, Y. Zhang, K. Watanabe, T. Taniguchi, D. Graf, A. F. Young, and C. R. Dean, Science **363**, 1059 (2019).
[27] C. Xu and L. Balents, Phys. Rev. Lett. **121**, 087001 (2018).
[28] G. Chen, A. L. Sharpe, P. Gallagher, I. T. Rosen, E. J. Fox, L. Jiang, B. Lyu, H. Li, K. Watanabe, T. Taniguchi, J. Jung, Z. Shi, D. Goldhaber-Gordon, Y. Zhang, and F. Wang, Nature (London) **572**, 215 (2019).
[29] C. Mora, N. Regnault, and B. A. Bernevig, Phys. Rev. Lett. **123**, 026402 (2019).

[30] A. Julku, T. J. Peltonen, L. Liang, T. T. Heikkilä, and P. Törmä, Phys. Rev. B **101**, 060505(R) (2020).

[31] J. M. Park, Y. Cao, K. Watanabe, T. Taniguchi, and P. Jarillo-Herrero, Nature (London) **590**, 249 (2021).

[32] J. Wang and Z. Liu, Phys. Rev. Lett. **128**, 176403 (2022).

[33] A. Himeda, T. Kato, and M. Ogata, Phys. Rev. Lett. **88**, 117001 (2002).

[34] F. Loder, A. P. Kampf, and T. Kopp, Phys. Rev. B **81**, 020511(R) (2010).

[35] P. A. Lee, Phys. Rev. X **4**, 031017 (2014).

[36] R. Soto-Garrido and E. Fradkin, Phys. Rev. B **89**, 165126 (2014).

[37] E. Fradkin, S. A. Kivelson, and J. M. Tranquada, Rev. Mod. Phys. **87**, 457 (2015).

[38] D. F. Agterberg, J. S. Davis, S. D. Edkins, E. Fradkin, D. J. Van Harlingen, S. A. Kivelson, P. A. Lee, L. Radzihovsky, J. M. Tranquada, and Y. Wang, Annu. Rev. Condens. Matter Phys. **11**, 231 (2020).

[39] Z. Han, S. A. Kivelson, and H. Yao, Phys. Rev. Lett. **125**, 167001 (2020).

[40] X. Liu, Y. X. Chong, R. Sharma, and J. C. S. Davis, Science **372**, 1447 (2021).

[41] T. Kitamura, A. Daido, and Y. Yanase, Phys. Rev. B **106**, 184507 (2022).

[42] W. Chen and W. Huang, arXiv:2208.02285.

[43] Here, we only consider superconducting states. The possibilities of other competing symmetry-broken states are beyond the scope of this work.

[44] B. A. Bernevig, T. L. Hughes, and S.-C. Zhang, Science **314**, 1757 (2006).

[45] X.-L. Qi, Y.-S. Wu, and S.-C. Zhang, Phys. Rev. B **74**, 085308 (2006).

[46] With our convention $\boldsymbol{q}$ is half of the center-of-mass momenta of the Cooper pairs in contrast to some literature.

[47] See Supplemental Material at http://link.aps.org/supplemental/10.1103/PhysRevLett.131.016002 for details of analytical and numerical calculations.

[48] E. Taylor, A. Griffin, N. Fukushima, and Y. Ohashi, Phys. Rev. A **74**, 063626 (2006).

[49] This choice of a Hermitian pairing matrix $\hat{\Delta}$ corresponds to a special type of spinful time-reversal symmetry, which has the operator form $\hat{\mathcal{I}}_s \otimes (-i\hat{s}_y K)$, with $\hat{\mathcal{I}}_s$ the identity matrix on the s-dim orbital space, $\hat{s}_y$ the Pauli matrix on spins, and K the complex conjugate operator.

[50] J. Provost and G. Vallee, Commun. Math. Phys. **76**, 289 (1980).

[51] R. Casalbuoni and G. Nardulli, Rev. Mod. Phys. **76**, 263 (2004).

[52] J.-X. Lin, P. Siriviboon, H. D. Scammell, S. Liu, D. Rhodes, K. Watanabe, T. Taniguchi, J. Hone, M. S. Scheurer, and J. I. A. Li, Nat. Phys. **18**, 1221 (2022).

[53] H. D. Scammell, J. I. A. Li, and M. S. Scheurer, 2D Mater. **9**, 025027 (2022).

[54] C. Huang, N. Wei, W. Qin, and A. H. MacDonald, Phys. Rev. Lett. **129**, 187001 (2022).

[55] M. Angeli and A. H. MacDonald, Proc. Natl. Acad. Sci. U.S.A. **118**, e2021826118 (2021).

[56] H. Chen *et al.*, Nature (London) **599**, 222 (2021).

[57] W. Ruan, X. Li, C. Hu, Z. Hao, H. Li, P. Cai, X. Zhou, D.-H. Lee, and Y. Wang, Nat. Phys. **14**, 1178 (2018).

[58] M. H. Hamidian, S. D. Edkins, S. H. Joo, A. Kostin, H. Eisaki, S. Uchida, M. J. Lawler, E.-A. Kim, A. P. Mackenzie, K. Fujita, J. Lee, and J. C. S. Davis, Nature (London) **532**, 343 (2016).

[59] Y. Yu, L. Ma, P. Cai, R. Zhong, C. Ye, J. Shen, G. D. Gu, X. H. Chen, and Y. Zhang, Nature (London) **575**, 156 (2019).